Determining through numerical modeling the effective thermal resistance of a foundation wall system with low emissivity materials and furred - airspace

NRCC-53574

Saber, H.H.; Swinton, M.C.

June 2010

A version of this document is published in / Une version de ce document se trouve dans:
ICBEST 2010 - International Conference on Building Envelope Systems and Technologies, Vancouver, B.C. June 27-30, 2010, pp. 247-257.

DETERMINING THROUGH NUMERICAL MODELING THE EFFECTIVE THERMAL RESISTANCE OF A FOUNDATION WALL SYSTEM WITH LOW EMISSIVITY MATERIAL AND FURRED – AIRSPACE

Hamed H. Saber and Michael C. Swinton
Heat and Moisture Performance of Envelopes,
Building Envelope and Structure Program
National Research Council Canada, Institute for Research in Construction (NRC-IRC)
Bldg. M-24, 1200 Montreal Road, Ottawa, Ontario, Canada K1A 0R6
http://irc.nrc-cnrc.gc.ca/irccontents.html

ABSTRACT
A numerical model was developed to investigate the effect of foil emissivity on the effective thermal resistance of a foundation wall system with foil bonded to expanded polystyrene foam in a furred assembly having airspace next to the foil. This model simultaneously solved the energy equation in the different material layers, surface-to-surface radiation equation in the furred – airspace assembly, and the coupled compressible Navier-Stokes equation and energy equation in the airspace. A parametric study was then conducted to determine the effective thermal resistance (R-value) of the foundation wall system as a function of foil emissivity. Consideration was also given to a accumulation of dust and condensation on the foil surface as these may also affect the emissivity of the foil. The results showed that when the furring was installed horizontally a low foil emissivity of 0.05 can increase the wall R-value to as much as ~10%. In the next phase of this work, the present model will be benchmarked against test results and it will also be used to determine the effective thermal resistance of foundation wall systems when the furring is installed vertically. The outcome of these efforts will be reported at a later date.

1. INTRODUCTION

Recently, a 2D and 3D hygrothermal model called "hygIRC-C" that uses COMSOL as a solver was developed at the National Research Council of Canada's Institute for Research in Construction (NRC-IRC). This model simultaneously solves the highly nonlinear 2D and 3D Heat, Air and Moisture (HAM) transport equations. These equations were discretized using the Finite Element Method (FEM). The use of the FEM provides an opportunity to model complicated wall geometries with less discretizing error. More recently, this model was benchmarked against the hygIRC-2D model that was previously developed at NRC-IRC [8 and 2] and test results in a number of client and strategic projects. Also, the 3D version of this model was used to conduct numerical simulations for different wall assembly configurations with and without through-wall penetrations to predict the effective thermal resistances (R-values) taking variations in air leakage of the assembly into account [3 and 4]. The predicted R-values for these

walls were in good agreement (within $\pm$ 5%) with the measured R-values in the NRC-IRC' Guarded Hot Box (GHB).

For foundation wall systems, airspace can contribute in obtaining a higher R-value, if a reflective material such as aluminum foil is installed on one side or the other of a furred-airspace. In respect to foundation wall systems having furred – airspace incorporating foil assemblies the question is: what might be the increase in R-value as function of the foil emissivity? The objective of this paper is to describe the approach adopted and results derived from a study on assessing the effective thermal resistance of foundation wall systems based on sensitivity analyses to investigate the effect of foil emissivity for foils laminated to expanded polystyrene (XPS) when used within a furred – airspace assembly.

Figure 1 shows an example of a 2438 mm x 2438 mm foundation wall system. The external layer of this wall normally should be poured-in-place concrete. However, not all laboratories may be in a position to test a wall specimen in GHB having a concrete layer. Alternatively, a plywood layer of 30 mm thick can be substituted for the concrete layer for the purposes of assessing the overall thermal resistance of the assembly in a steady-state condition (i.e. no mass effect). In the numerical simulations, a plywood layer was also used to replace the concrete layer in order to benchmark the present model against the experimental data when it is available. In this paper, four furring strips made of spruce (19 mm x 38 mm) were installed horizontally (Figure 1). In foundation wall systems, however, furring of different sizes (19 mm x 38 mm or 19 mm x 64 mm) can be installed either horizontally or vertically. It must be considered that the thermal resistance of the foundation wall system can not only be affected by the number and size of the furring strips, but also the orientation of the strips. The mode of heat transfer through the different solid layers of the foundation wall systems is by conduction. Whereas in the airspaces within the assembly, the modes of heat transfer are by conduction, convection, and radiation as discussed next.

2. PROBLEM DESCRIPTION

A schematic of a furred – airspace within a foundation wall assembly is shown in Figure 2. It is assumed that the indoor temperature is greater than the outdoor temperature. As shown in this figure, there are three modes of heat transfer in the airspace, namely:

(a) Radiation: A net radiative heat is transferred from the hot surface (gypsum board) to the cold surface (foil/XPS);

(b) Conduction: A net conductive heat is transferred from the hot surface to the cold surface, and;

(c) Convection: Since the gypsum board surface has a higher temperature than the foil/XPS surface, and taking into consideration the buoyancy effect, the air adjacent to the former moves upward, while the air adjacent to the latter moves downward, resulting in convection current that in turn increases the heat transfer in the airspace enclosure.

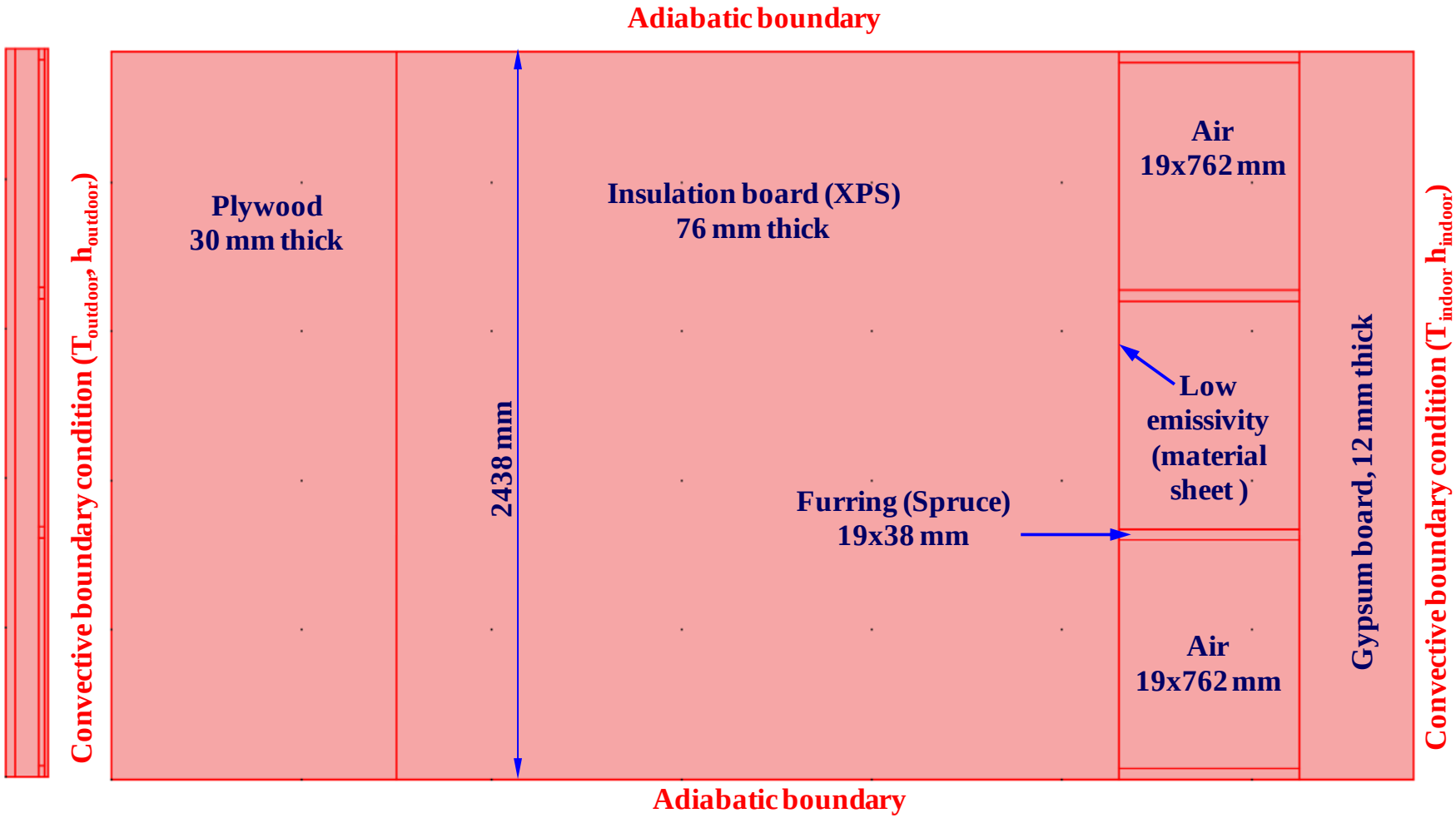

Figure 1 - An example of a foundation wall with multiple enclosures

The contributions of the three modes of heat transfer (radiation, conduction and convection) result in a higher equivalent thermal conductance of the airspace enclosure than that of a vacuum. As described in the next section, in order to model the heat transfer by radiation, convection and conduction in the airspace (see Figure 1), the energy equation in the solid material layers, surface-to-surface heat radiation equation in the furred – airspace assembly, and the coupled compressible Navier-Stokes equation with energy equation in the airspace are all solved simultaneously. In the meantime, the opacity of the airspace must be considered as transparent so that the radiation rays from the surface boundaries are not blocked. Since there is no radiation through the solid material layers, they are treated as opaque bodies.

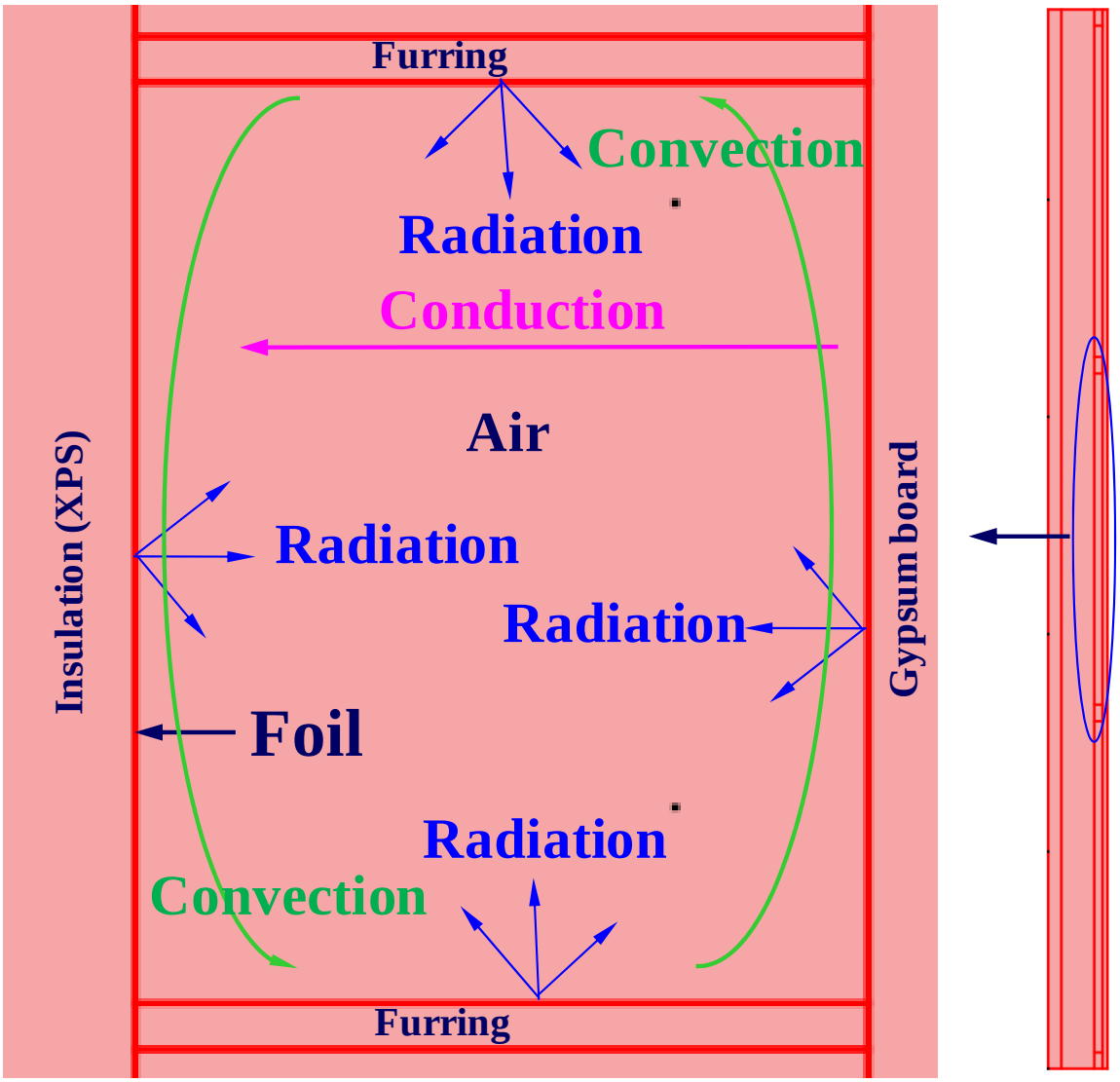

Figure 2 - Modes of heat transfer in furred-airspace assembly

3. GOVERNING EQUATIONS

The present model solves the governing equations that are described in the following subsections.

Continuity and Momentum Equations

In the airspace, the air velocity field, $\vec{v}_a$, and pressure field, P_a, is calculated by solving the continuity equation and momentum equation (compressible Navier-Stokes equation). These equations are respectively given as [5]:

$$\frac{\partial \rho_a}{\partial t} = -\left(\nabla \bullet \left(\rho_a \vec{v}_a\right)\right), \text{ and} \tag{1}$$

$$\rho_a \frac{\partial \vec{v}_a}{\partial t} + \rho_a \vec{v}_a \bullet \nabla \vec{v}_a = -\nabla P_a + \rho_a \vec{g} + \nabla \bullet \left(\mu_a \left(\nabla \vec{v}_a + (\nabla \vec{v}_a)^T\right) - \frac{2}{3}\mu_a \left(\nabla \bullet \vec{v}_a\right) I \right). \tag{2}$$

In porous materials, the continuity and momentum equations are respectively given as [5]:

$$\varepsilon_o \frac{\partial \rho_a}{\partial t} = -\left(\nabla \bullet \left(\rho_a \vec{v}_a\right)\right), \text{ and} \tag{3}$$

$$\text{Darcy's law: } \vec{v}_a = -\frac{\kappa_a}{\mu_a}\left(\nabla P_a - \rho_a \vec{g}\right). \tag{4}$$

Energy Equation

The energy equation in the airspace is given as:

$$\rho_a Cp_a \frac{\partial T}{\partial t} = -\underbrace{\rho_a Cp_a (\vec{v}_a \bullet \nabla T)}_{\text{convection}} + \underbrace{\nabla \bullet (\lambda_a \nabla T)}_{\text{conduction}}$$
$$+ \underbrace{\eta_a \left(\left(\nabla \vec{v}_a + (\nabla \vec{v}_a)^T\right) - \frac{2}{3}\left(\nabla \bullet \vec{v}_a\right) I \right) : \nabla \vec{v}_a}_{\text{viscous heating}} \quad \underbrace{-\frac{T}{\rho_a}\frac{\partial \rho_a}{\partial T}\bigg|_p \left(\frac{\partial P_a}{\partial t}\right)}_{\text{Pressure work}} + q'''_{\text{source/sink}} . \tag{5}$$

Where $q'''_{\text{source/sink}}$ represents the heat source/ sink (e.g. due to condensation/evaporation), which is neglected since no moisture transport was considered in this work. In typical building applications, the contribution due to pressure work and viscous heating are much smaller than that due to convection and conduction. Neglecting these terms in Eq. (5), the resulting energy equation becomes:

$$\rho_a Cp_a \frac{\partial T}{\partial t} = -\rho_a Cp_a (\vec{v}_a \bullet \nabla T) + \nabla \bullet (\lambda_a \nabla T). \tag{6}$$

In porous materials, the energy equation is:

$$\rho_m Cp_m \frac{\partial T}{\partial t} = -\rho_a Cp_a (\vec{v}_a \bullet \nabla T) + \nabla \bullet (\lambda_m \nabla T). \quad (7)$$

The surface-to-surface heat radiation equation for the furred – airspace assembly (derived in the next section) coupled with Eqs. (1), (2) and (6) in the airspace, and Eqs. (3), (4) and (7) in the porous material layers are solved simultaneously at the steady-state condition for pressure, P_a, velocity, $\vec{v}_a$, and temperature, T.

Radiative Heat Flux Equation in Enclosure

This section describes the theory behind the radiative heat transfer process in the building envelope. Thermal radiation denotes the stream of electromagnetic waves emitted from a body at a certain temperature. For opaque surfaces, no radiation is transmitted through the body. The incoming radiative heat flux at a location on the surface is called the irradiation, q_{irr}. A portion of the irradiation is reflected from the surface. This portion depends on the surface reflectivity, ρ_r. Additionally, the surface emits a thermal flux that depends on both its emissivity, ε, and temperature, T_s. The total outgoing radiative heat flux at this location is called the radiosity, q_{radi}. The radiosity is the sum of the reflected radiation and emitted radiation from the surface, which is given as:

$$q_{radi} = \rho_r \, q_{irr} + \varepsilon \, \sigma \, T_s^4. \quad (8)$$

The net inward radiative heat flux, q_{RAD}, is the difference between the irradiation and radiosity:

$$q_{RAD} = q_{irr} - q_{radi} = (1 - \rho_r) \, q_{irr} - \varepsilon \, \sigma \, T_s^4. \quad (9)$$

In the building envelope, most opaque bodies behave as gray bodies. As such, the long wave absorptivity, α, and emissivity are equal, and the reflectivity, ρ_r, is therefore given as:

$$\rho_r = 1 - \varepsilon = 1 - \alpha. \quad (10)$$

From Eqs. (9) and (10), the net inward radiative heat flux for gray bodies is given as:

$$q_{RAD} = q_{irr} - q_{radi} = \varepsilon \left(q_{irr} - \sigma \, T_s^4 \right). \quad (11)$$

Surface-to-surface radiation is complex as mutual radiation from all adjacent surfaces must be taken into consideration when determining the net radiative flux at any given surface. Consider the case of an enclosed space with no openings, as, for example, the instance of a furred – airspace assembly in a foundation wall system. However, in the case of enclosure with opening(s) to the ambient surroundings (see Figure 3), it includes radiation from both the ambient surroundings and from other surfaces.

To derive a general expression for surface-to-surface radiation, consider an enclosure with an opening to ambient surroundings as shown in Figure 3. This enclosure is formed from different surfaces with different materials. Consider an infinitesimal surface area dA of a target located at arbitrary point h on the surface S_4 of material mat_4. This point can see points on the other surfaces and the ambient surroundings as well. Each point on all surfaces has a local radiosity,

$q'_{radi}(\vec{r}')$. Assume the ambient surroundings have a constant emissivity, ε_{amb}, and temperature, T_{amb}. The mutual irradiation, G_m, at an arbitrary point h is given by the following surface integrals as [6]:

$$G_m = \sum_{i=1}^{m} \int_{S_i} K_S(\vec{r},\vec{r}')\, q'_{radi}(\vec{r}')\, dS \text{ , m = number of surfaces.} \tag{12}$$

Where $K_S(\vec{r},\vec{r}')$ is the kernel function, which for a 3D problem is given as [6]:

$$K_S(\vec{r},\vec{r}') = \frac{\left(-\vec{n}'\bullet\left(\vec{r}-\vec{r}'\right)\right)\left(\vec{n}\bullet\left(\vec{r}-\vec{r}'\right)\right)}{\pi\left|\vec{r}-\vec{r}'\right|^4}\chi. \tag{13}$$

In Eq. (13), the parameter χ has a value of 1.0 when the infinitesimal surface area dA at the target (point h) sees the infinitesimal surface area dA' at the source (point d) as illustrated by the ray connecting points h to d (i.e. $\vec{r}-\vec{r}'$), and otherwise it is 0 if the ray $\vec{r}-\vec{r}'$ is blocked (see Figure 3). Note that for a given surface the parameter χ can have a value of 1.0 on a portion of this surface and 0 on the other portion of this surface. For example, for a target located at point h as shown in Figure 3, the parameter χ for the surface S_1 has a value of 1.0 on the portion of this surface from b to c, and a value of 0 on the portion from a to b.

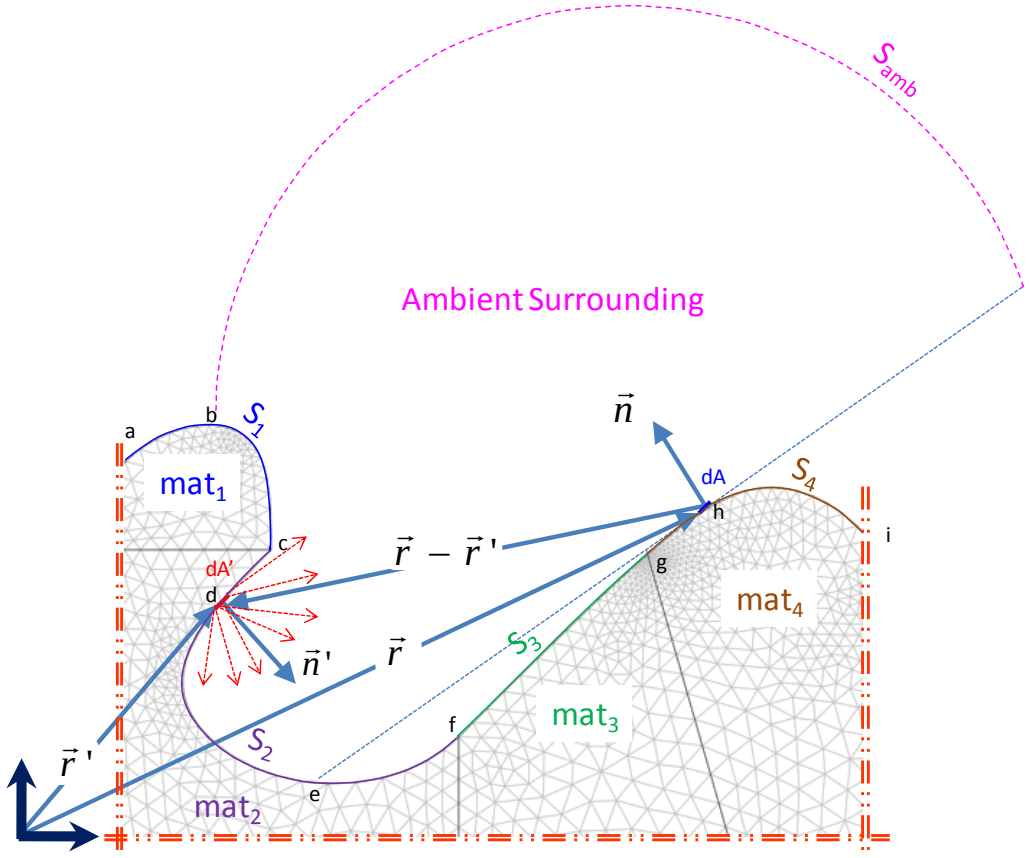

Figure 3 - A schematic of surface-to-surface radiation for enclosure with opening to ambient

In order to account for the mutual irradiation due to the ambient surroundings at a target located at point h, the ambient view factor, F_{amb}, needs to be determined as follows:

$$F_{amb} = 1 - \sum_{i=1}^{m} F_{S_i}, \text{ with } F_{S_i} = \int_{S_i} K_S(\vec{r}, \vec{r}')\, dS. \tag{14}$$

In the case of a 2D problem, the mutual irradiation at point h is given by the following the line integrals as:

$$G_m = \sum_{i=1}^{m} \int_{L_i} K_L(\vec{r}, \vec{r}')\, q'_{radi}(\vec{r}')\, dL, \tag{15}$$

m = number of line boundaries.

Where the kernel function for a 2D problem is given as [6]:

$$K_L(\vec{r}, \vec{r}') = \frac{\left(-\vec{n}' \bullet \left(\vec{r} - \vec{r}'\right)\right)\left(\vec{n} \bullet \left(\vec{r} - \vec{r}'\right)\right)}{2\left|\vec{r} - \vec{r}'\right|^3} \chi. \tag{16}$$

The ambient view factor in the case of 2D geometry is given as:

$$F_{amb} = 1 - \sum_{i=1}^{m} F_{L_i}, \text{ with } F_{L_i} = \int_{L_i} K_L(\vec{r}, \vec{r}')\, dL. \tag{17}$$

The general equation for the total irradiative heat flux arriving at a target at an arbitrary point on a surface (3D geometry) or line boundary (2D geometry) can now be obtained by summing up the contribution of the mutual irradiation from all surfaces (3D geometry) or all line boundaries (2D geometry), and the ambient surroundings as follows:

$$q_{irr} = G_m + F_{amb}\, \varepsilon_{amb}\, \sigma\, T_{amb}^4. \tag{18}$$

In the case of a 3D problem, G_m and F_{amb} are given by Eqs. (12) and (14), respectively. Whereas, in the case of a 2D problem, G_m and F_{amb} are given by equations (15) and (17), respectively. For an enclosure with no openings to ambient surroundings, the last term on the right hand side of Eq. (18) is zero (since $F_{amb} = 0$).

In the building envelope, a given problem may have more than one enclosure. Figure 1 shows an example of multiple airspaces for a foundation wall system with horizontal furring. Each airspace shown in this figure is bounded by furring (spruce), gypsum board and a low emissivity sheet of material.

After deriving the expression for the total irradiation arriving at an arbitrary point on a surface (3D geometry) or a line boundary (2D geometry), q_{irr} (Eq. (18)), the radiosity emitted from this point can now be calculated by substituting the value of q_{irr} from Eq. (18) into Eq. (11):

$$q_{radi} = (1-\varepsilon)\left(G_m + F_{amb}\ \varepsilon_{amb}\ \sigma\ T_{amb}^4\right) + \varepsilon\ \sigma\ T_s^4 . \quad (19)$$

The above equation is applicable to all points on the surface/line boundaries that participate in surface-to-surface radiation. This equation forms a system of equations in radiosity q_{radi}. This system of equations is solved simultaneously with the energy equation (Eqs. (6) and (7)) for the temperature, T and radiosity q_{radi}.

4. RESULTS AND DISCUSSIONS

In the numerical simulations, the emissivity of all materials of the wall specimen was assumed equal to 0.8. The emissivity of aluminum foil is normally less than 0.1. However, the accumulation of dust (e.g. due to construction) and condensation on the foil surface can cause an increase in the foil emissivity. In order to investigate the effect of the foil emissivity on the wall R-value, the numerical simulations were conducted for different values of foil emissivity ranging from 0 – 0.8. The case of high foil emissivity (e.g. 0.8) may represent the case of: (a) no foil installed in the wall system, or; (b) a significant portion of the foil surface covered by dust and/or thin film of water due to condensation.

When assessing the effective R-value of the foundation wall with the foil installed on the surface of the insulation two competing effects must be considered, namely:
(a) The net radiative heat flux from the surfaces of furring and gypsum board to the surface of foil is lower in the case of foil with low emissivity than that in the case of foil with high emissivity, resulting in an increase in wall R-value with low foil emissivity. This is a positive effect on the wall R-value.
(b) The temperature difference across the airspace is larger in the case of foil with low emissivity (due to low net radiative heat flux) than that in the case of foil with high foil emissivity. As such, the convection current of the air inside the airspace becomes stronger in wall with lower emissivity, resulting in an increase in the heat transfer in the airspace due to convection. This is a negative effect on the wall R-value. As will be shown later, the two interactive and competing effects result in a net increase in the effective R-value of a wall having a foil of low emissivity as compared to a wall with a foil of high emissivity.

Figure 4(a) and (b) show the temperature contours (in ^oC) at steady-state condition in a portion around a furring of the wall specimen with foil emissivity of 0.05 and 0.8, respectively, in the case of the indoor temperature of $+20^oC$ and outdoor temperature of -20^oC ($\Delta T_{amb} = 40^oC$). Also, Figure 5(a) and (b) show the temperature contours in the furred – airspace assembly and gypsum board with foil emissivity of 0.05 and 0.8, respectively. As shown in this figure, the temperature gradient across the airspace with foil emissivity of 0.05 is greater than that with foil emissivity of 0.8.

Figure 6(a) and (b) show the vertical velocity contours (in mm/s) in the airspace for the wall assembly having a foil emissivity of 0.05 and 0.8, respectively. Because the temperature of the gypsum board is higher than the temperature of the foil surface (see Figure 4 and Figure 5), the air adjacent to the former travels upward while the air adjacent to the latter travels downward, forming convection currents (loops) inside the airspace as shown in Figure 6. Note that the

degree of convective heat transfer increases with higher air velocity in the airspace. As expected, both the upward and downward vertical velocities of the air are considerably higher in the wall having a foil with emissivity of 0.05 (Figure 6(a)) as compared to a wall having a foil with emissivity of 0.8 (Figure 6(b)).

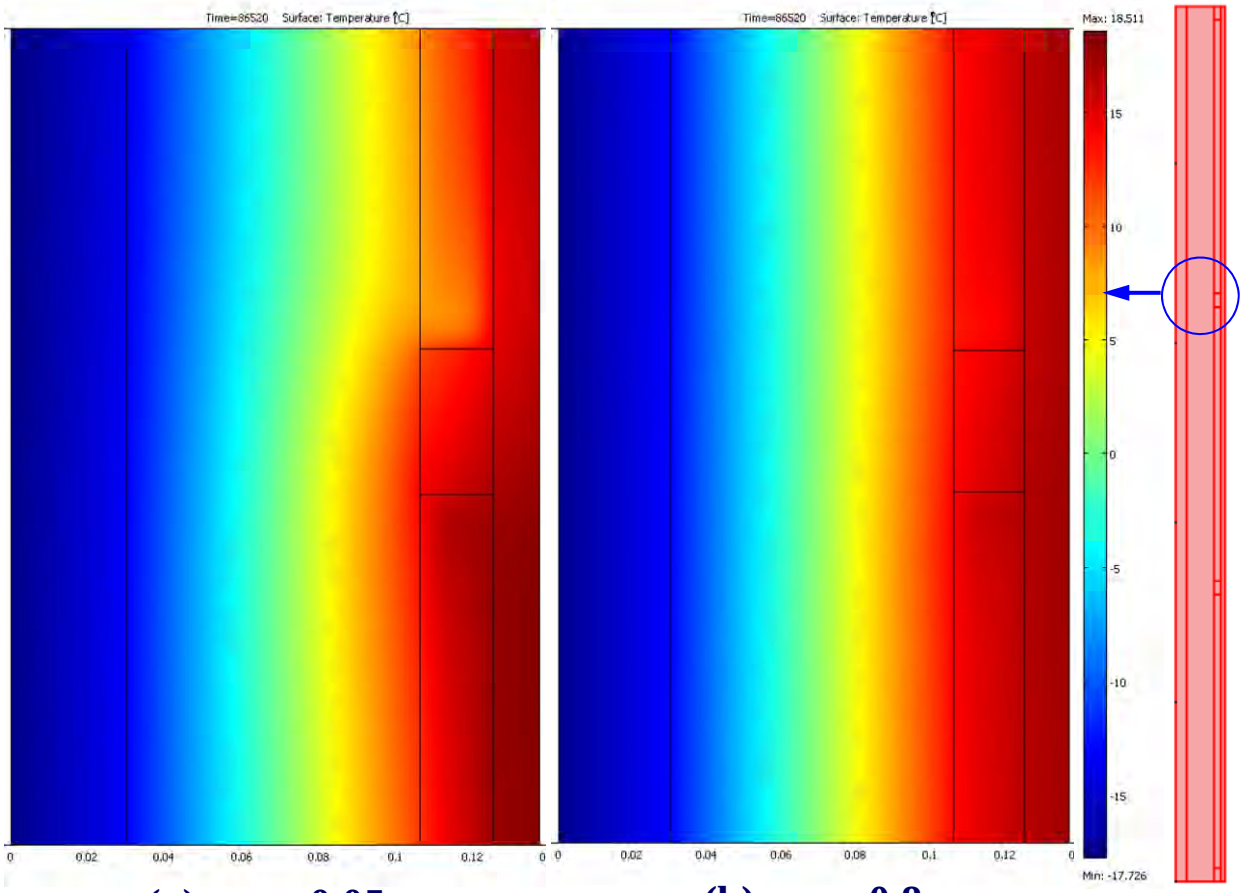

Figure 4 - Temperature contours (in ^{o}C) in wall specimen with foil emissivity of (a) 0.05 and (b) 0.8 ($\Delta T_{amb} = 40^{o}C$).

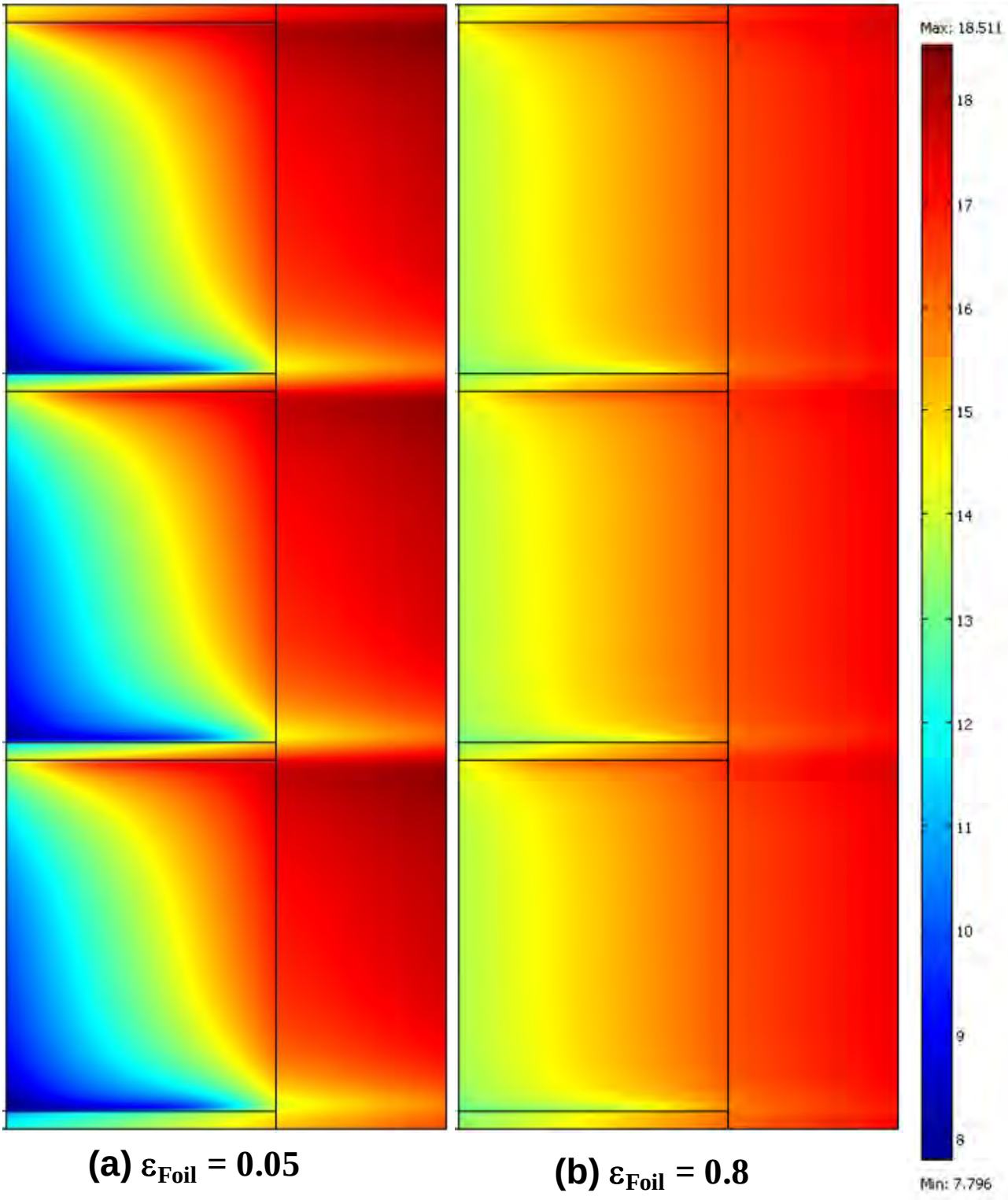

Figure 5 - Temperature contours (in ^{o}C) in the furred – airspace assembly and gypsum board with foil emissivity of (a) 0.05 and (b) 0.8 (ΔT_{amb} = 40^{o}C).

In Figure 7 at section A-A through the airspace , the maximum upward air velocity in wall with foil emissivity of 0.05 is 41.3 mm/s, which is ~2.3 times the maximum upward air velocity of a wall with foil emissivity of 0.8 (17.8 mm/s). Additionally, the maximum downward air velocity in wall with foil emissivity of 0.05 is -38.5 mm/s compared to -17.5 mm/s for a wall with foil emissivity of 0.8 (Figure 7(a)). As such, the reduction in the R-value due to convective heat transfer in the airspace for the wall with foil emissivity of 0.05 is greater than that for the wall with foil emissivity of 0.8. Furthermore, due to low radiative heat flux in the case of low foil emissivity, the temperature difference across the airspace at section A-A ((Figure 7(b)) is 6.6^{o}C for the wall with foil emissivity of 0.05, which is about ~2.4 times the temperature difference across the airspace for wall with foil emissivity of 0.8 (2.7^{o}C).

In order to illustrate the effect of the three modes of heat transfer in the airspace (conduction, convection and radiation) and the effect of thermal bridges due the furring on the thermal response of the wall in the case of different foil emissivities (0.05 and 0.8), Figure 8(a) and (b) show the local temperature distribution on the outer and inner surfaces of the gypsum board, respectively. As shown in this figure, in the lower portions of the airspaces where the downward cold air (close to the foil surface) is circulated so as to move upward (close to the inner surface of the gypsum board), it absorbs heat from the surface of the gypsum board, resulting in a decrease in its temperature in this portion (see Figure 8). Additionally, because the air velocity of the convection currents in the case of foil emissivity of 0.05 is greater than that in the case of foil emissivity of 0.8 (see Figure 7(a)), the amount of heat absorbed by this cold air from the gypsum board is higher in the case of low foil emissivity. As such, the minimum temperature of the inner surface of the gypsum board is smaller in the case of low foil emissivity (14.2^{o}C) than that in the case of high foil emissivity (15.8^{o}C). In the meantime, the heat absorbed by the air from the gypsum board in the lower portion of the airspace increase the air temperature. While the air close to the surface of gypsum board travels upward, its ability to absorb additional heat from the gypsum board deceases, resulting in an increase in the temperature of the gypsum board (see Figure 8).

At a height of ~170 mm above the furring, the inner surface temperatures of the gypsum board are equal for either type of foil (i.e. foil having emissivities of 0.05 and 0.8). In the case of the foil with the lower emissivity, the gypsum board attains a higher temperature at heights above the furring in excess of 170 mm (i.e. >170 mm). For example, within the airspace located at the bottom of the wall, the maximum temperature of the inner surface of the gypsum board reaches 17.8^{o}C in the case of the foil with emissivity of 0.05 as compared to 16.7^{o}C for the foil of emissivity 0.8 (Figure 8(b)). Finally, as shown in Figure 8, in the case of the foil with emissivity of 0.05, the average temperature of the inner and outer surfaces of the gypsum board (16.7^{o}C and 17.6^{o}C, respectively) are higher than that the foil with emissivity of 0.8 (16.4^{o}C and 17.4^{o}C, respectively).

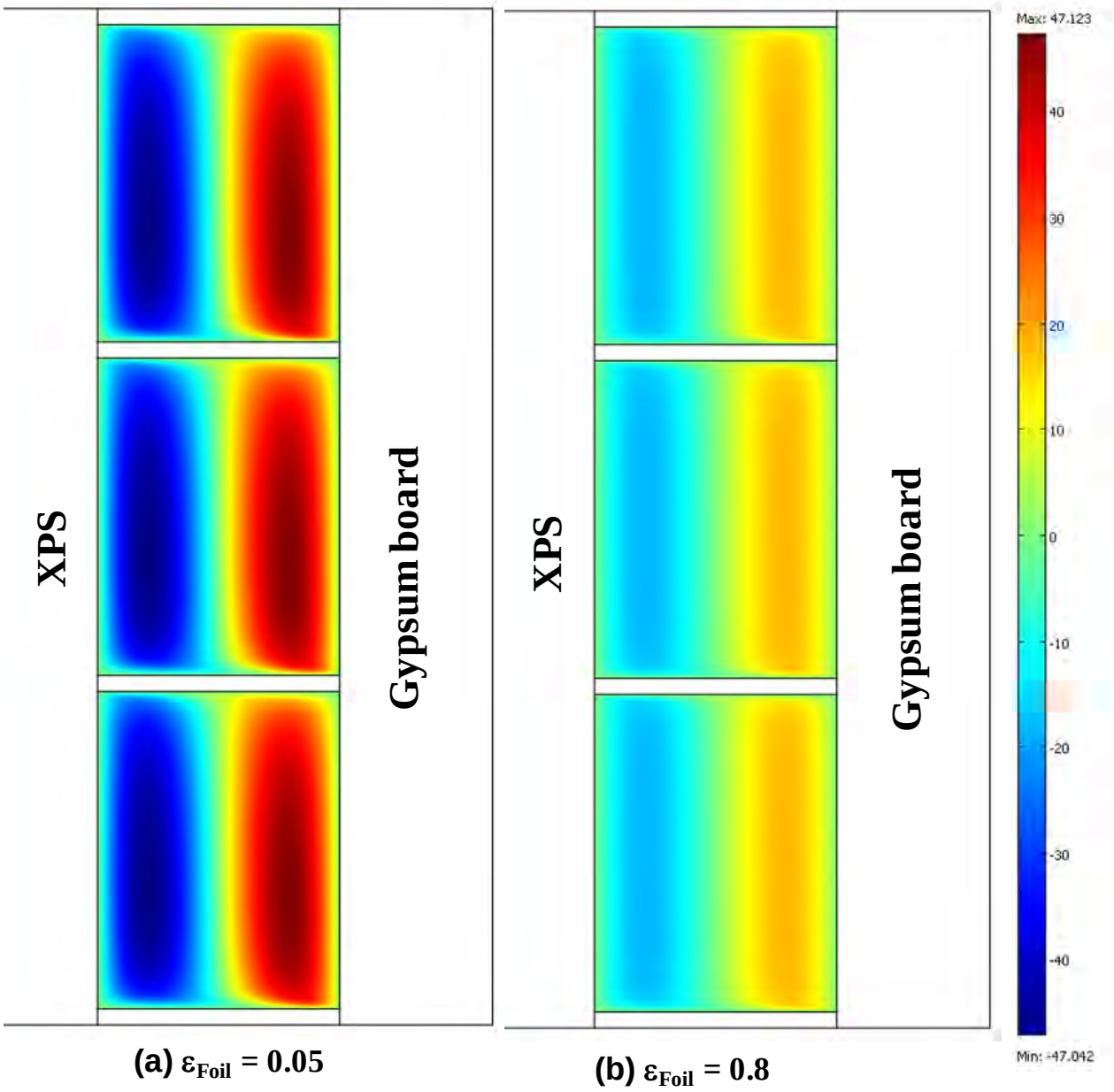

(a) ε_{Foil} = 0.05 **(b) ε_{Foil} = 0.8**

Figure 6 - Vertical velocity contours (in mm/s) in the airspaces with emissivity of (a) 0.05 and (b) 0.8 (ΔT_{amb} = 40°C).

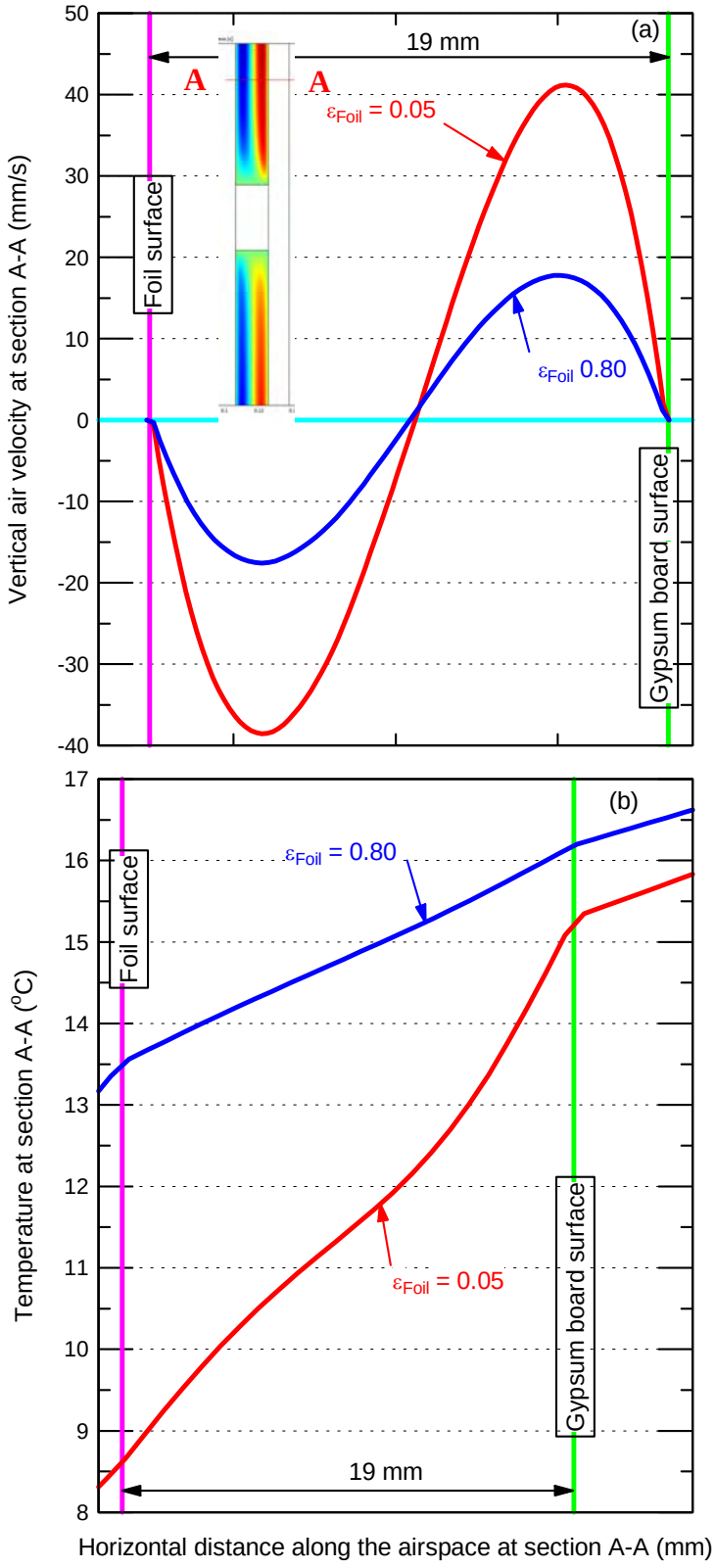

Figure 7 - Vertical velocity and temperature distribution across the airspace at section A-A

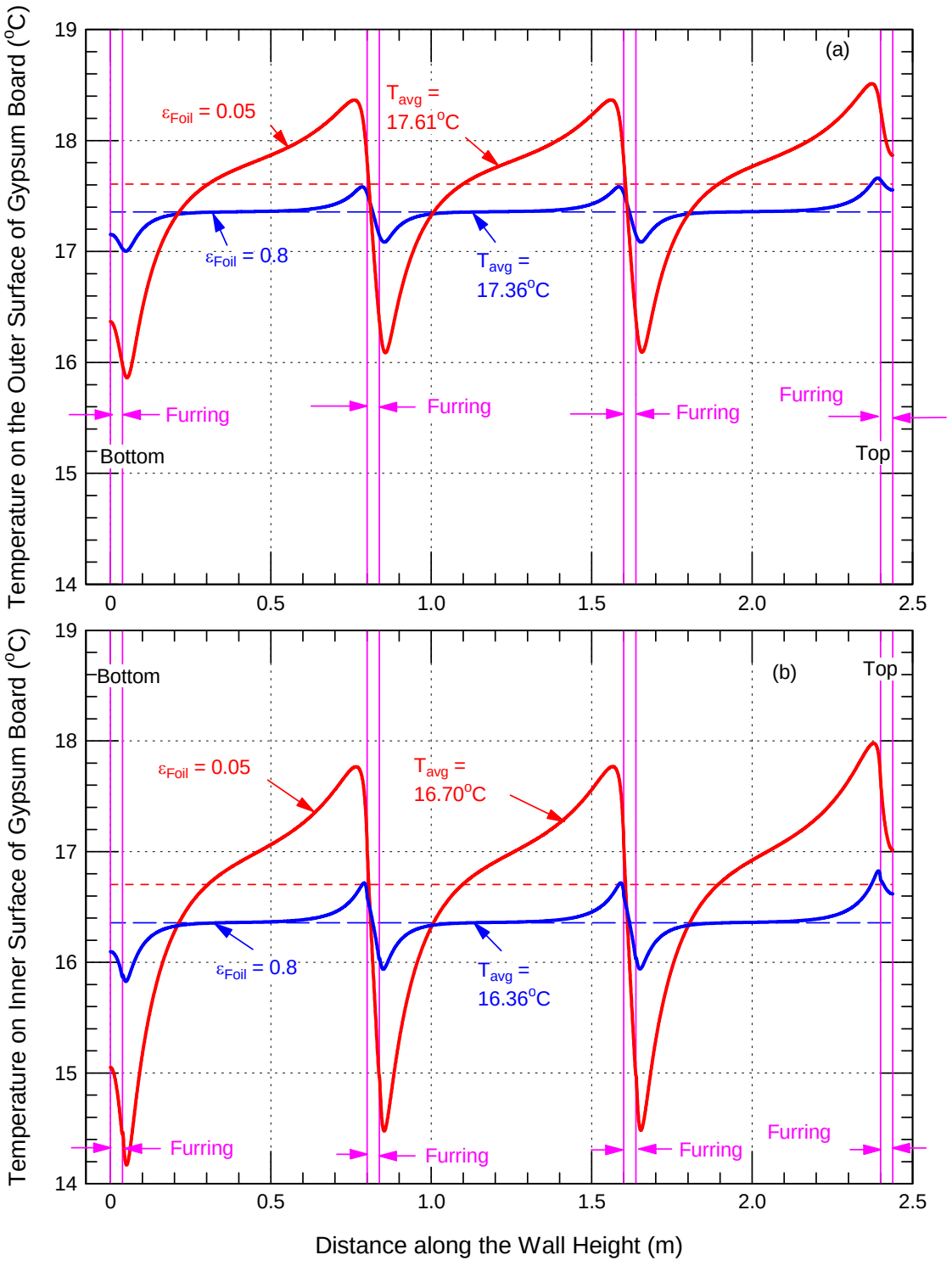

Figure 8 - Comparison of temperature on the outer and inner surfaces of gypsum board with foil emissivity of 0.05 and 0.8.

Figure 9 shows the effect of foil emissivity on the effective R-values of wall foundation system when the difference between the indoor and outdoor temperature, ΔT_{amb}, is 40°C and 60°C. For the same foil emissivity, a larger ΔT_{amb} results in a larger net radiative heat flux and stronger convection currents in the airspace than that for smaller ΔT_{amb}. As such, the wall R-value with larger ΔT_{amb} is less than that of the wall with smaller ΔT_{amb}. For example, for a foil emissivity of 0.05, the wall R-values with ΔT_{amb} of 60°C and 40°C were 3.51 and 3.55 m^2K/W, respectively (Figure 9(a)).

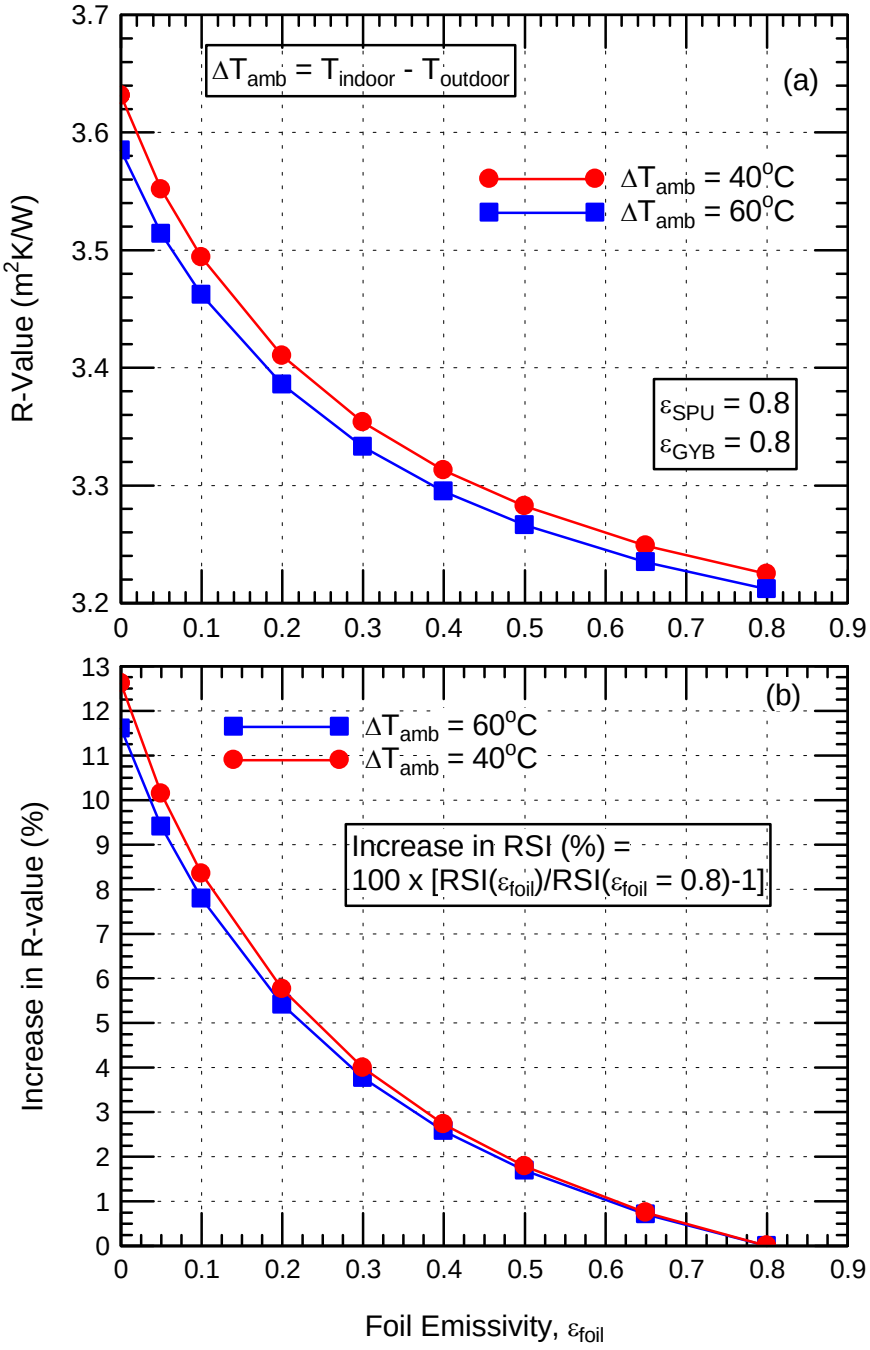

Figure 9 - Effect of foil emissivity on the effective R-value

As mentioned earlier, the foil emissivity can increase due to accumulation of dust and/or condensation on the foil surface. Figure 9(a) show that in the range of foil emissivity of 0 – 0.4, the wall R-value decreases considerably as the foil emissivity increases. In the range of foil emissivity of 0.4 – 0.8, however, the wall R-value slowly decreases as the foil emissivity increases. For example, at ΔT_{amb} = 40°C, the wall R-value decreases by 0.32 m^2K/W, and 0.09 m^2K/W as the foil emissivity increases from 0 to 0.4, and from 0.4 to 0.8, respectively.
The results of the wall R-values shown in Figure 9(a) were normalized so as to determine the percentage increase in the R-value as a function of foil emissivity (see Figure 9(b)). In this normalization, a wall with foil emissivity of 0.8 was used as a reference, which approximately represent the case of no foil installed in the wall system or significant portion of the foil surface is covered by thin water film due to condensation. Figure 9(b) shows that as the foil emissivity increases, the "percentage increase in the R-value" decreases. Moreover, as shown in Figure 9(b), a wall with foil emissivity of 0.05 has an increase in R-value by 10.14% and 9.40% for ΔT_{amb} of 40°C and 60°C, respectively.

5. SUMMARY AND CONCLUSIONS

The present model, hygIRC-C, was used to conduct numerical simulations to determine the effective thermal resistance of a foundation wall system having a furred – airspace assembly and incorporating low emissivity foil materials. This model accounts for surface-to-surface radiation between the surfaces of the furring, gypsum board and foil. In order to account for the conductive, convective and radiative heat transfer in the furred – airspace assembly, the energy equation in the different material layers, surface-to-surface radiation equation in the furred – air assembly, and the coupled compressible Navier-Stokes equation and energy equation in the airspace were solved simultaneously at steady-state conditions. Results showed that a foil with lower emissivity has two interactive and competing effects on the R-value of the wall, namely: (i) an increase in wall R-value due to lower net radiative heat flux in the furred – airspace assembly, and (ii) a decrease in R-value due to stronger convection currents in the airspace. The former effect outweighs the latter, resulting in a net increase in the effective R-value for a wall system with low foil emissivity. Additionally, the results showed that the modelled foundation wall system with foil of emissivity 0.05 increased the effective R-value by about 10%. In future publications, the authors will describe the benchmarking of the present model against experimental data recently generated by an independent laboratory and applied to basement wall systems having multiple airspaces.

6. ACKNOWLEDGMENTS

The authors wish to thank Caroline St-Onge from Canadian Construction Materials Center (CCMC) for her feedback and discussion about this work, and Wahid Maref from Building Envelope and Structure Program for reviewing this paper.

7. NOMENCLATURES

Cp Specific heat (J/(kg K))
$\vec{g}$ vector of gravitational acceleration (m^2/s)

I 3x3 unit matrix
$\vec{n}$ normal vector at the target (point h)
$\vec{n}'$ normal vector at the sources (point d)
P pressure (Pa)
$\vec{r}$ vector points from the origin to the target (point h)
$\vec{r}'$ vector points from the origin to the source (point d)
$\vec{r} - \vec{r}'$ vector points from the source (point d) to the target (point h)
$\vec{v}$ velocity vector (m/s)
T temperature (K)
t time (s)

Greek Symbols

ε porosity
ρ density (kg/m^3)
σ Stefan-Boltzmann constant, 5.67E-8 W/(M^2 K^4)
μ dynamic viscosity (Pa·s)
κ permeability (m^2)
λ thermal conductivity (W/(m·K))
χ parameter equal to 0 or 1.0

Subscripts

a air
m solid
s surface

8. REFERENCES

1. Maref, W., Kumaran, M.K., Lacasse, M.A., Swinton, M.C., van Reenen, D. "Laboratory measurements and benchmarking of an advanced hygrothermal model," Proceedings of the 12th International Heat Transfer Conference (Grenoble, France, August 18, 2002), pp. 117-122, October 01, 2002 (NRCC-43054).
2. Maref, W., Lacasse, M.A., Kumaran, M.K., Swinton, M.C. "Benchmarking of the advanced hygrothermal model-hygIRC with mid-scale experiments," eSim 2002 Proceedings (University of Concordia, Montreal, September 12, 2002), pp. 171-176, October 01, 2002 (NRCC-43970).
3. Elmahdy, A.H., Maref, W., Swinton, M.C., Saber, H.H., Glazer, R. “Development of Energy Ratings for Insulated Wall Assemblies” 2009 Building Envelope Symposium (San Diego, CA. 2009-10-26) pp. 21-30, 2009.
4. Saber, H.H., Maref, W., Elmahdy, A.H., Swinton, M.C., and Glazer, R. “3D Hygrothermal Model for Predicting the Thermal Resistances of Spray Polyurethane Foam Wall Assemblies”, submitted to Building XI conference, Clearwater, Florida, 2010.
5. Bird, R. B., Stewart, W. E., and Lightfoot, E. N., Transport Phenomena, John Wiley & Sons, Inc., 1960.
6. Siegel, R., and Howell, J.R. Thermal Radiation Heat Transfer (3rd edition), Hemisphere Publishing Company: Washington, DC, 1992.